

# Metadata of the chapter that will be visualized in SpringerLink

Book Title	Nano-tribology and Materials in MEMS	
Series Title		
Chapter Title	Nanotribology and Wettability of Molecularly Thin Film	
Copyright Year	2013	
Copyright HolderName	Springer-Verlag Berlin Heidelberg	
Corresponding Author	Family Name	<b>Wang</b>
	Particle	
	Given Name	<b>Liping</b>
	Suffix	
	Division	State Key Laboratory of Solid Lubrication, Lanzhou Institute of Chemical Physics
	Organization	Chinese Academy of Sciences
	Address	730000, Lanzhou, P. R. China
	Email	lpwang@licp.cas.cn
Author	Family Name	<b>Mo</b>
	Particle	
	Given Name	<b>Yufei</b>
	Suffix	
	Division	State Key Laboratory of Solid Lubrication, Lanzhou Institute of Chemical Physics
	Organization	Chinese Academy of Sciences
	Address	730000, Lanzhou, P. R. China
	Email	
Abstract	<p>The micro/nano-electromechanical systems (MEMS/NEMS) have received rapid development in the past decades due to their superior performance and low unit cost. However, large surface area-to-volume ratio causes serious adhesive and frictional problems for MEMS operations. Nanotribology is a study of the interaction between contact surfaces at nanoscale, from chemistry and physics to material science and mechanical engineering, and is of extreme technological importance to the application and development of MEMS. This chapter will attempt to cover the range from preparation of organic thin films to instruments and measurement protocols. We will describe this process in steps. The preparation of thin film materials (i.e., ionic liquids, multiply-alkylated cyclopentane or self-assembled molecules) and film deposition are presented. Also, the methods of film evaporation are considered. We examined the relationship of adhesion and lateral force data to their fundamental aspects at molecular level. The main objective will be to provide more thorough examination to the interested reader, and to provide a source to further raise the critical issues concerning the relationship between surface properties and MEMS application. Fluorinated molecules with coplanar structure were successfully self-assembled onto silicon surface. The fluorinated monolayers possessed excellent adhesion-resistance, friction-reduction and anti-wear durability, which were attributed to low interfacial energy of end group and dual layer structure of the films. The spatial distribution of the multi-component film was evaluated by adhesion statistic measurement. Multialkylated cyclopentanes (MACs) are potential lubricants for space and MEMS application due to their extreme low volatility. A series of MACs were synthesized by Dean-Stark trap, autoclave, and phase transfer catalysis methods. Nanoscale dual-layer films consisting of both MACs and self-assembled monolayers (SAMs) were prepared and their morphology, wettability and tribological properties were investigated. Molecularly thin ILs films with different molecular structures which showed excellent tribological performance were designed, synthesized and prepared successfully on silicon surface by dip-coating method. The influences of anion, cation and post-treatment on wettability and tribological properties of ILs films were investigated</p>	

systematically. To enhance the wettability and to improve the nanotribology of nano films, surface texture technique is reviewed. Regular and biomimetic surface textures were fabricated by local anodic oxidation (LAO). Dimension of the pillars were precisely controlled by operation parameters such as pulse bias voltage, pulse width and humidity. The H-passivated Si showed higher growth rate and thicker saturated oxide film than common p- or n-type Si under the same oxidation condition. The H-passivated Si employed in LAO process can improve lateral resolution of patterns. The adhesive and friction force of LAO pattern were measured by AFM colloidal probe. The friction forces are closely related to the surface coverage of the nanotexture. The results indicate that nanotextures significantly reduced the friction force, while H-passivated Si showed large friction force, this is because of the less adhesive energy dissipated during sliding on textured surface. The surface nanotextures of biological origins were fully duplicated on surface based on duplication method. The morphology and the size of the surface textures of the replicas are almost in accordance with their biological sources. The wettability of the surfaces was improved with hydrophobicity after duplicating with textures. And the biomimetic textures have shown to improve nanotribological performance.

---



1 **Chapter 3**  
2 **Nanotribology and Wettability**  
3 **of Molecularly Thin Film**

4 **Yufei Mo and Liping Wang**

5 **Abstract** The micro/nano-electromechanical systems (MEMS/NEMS) have  
6 received rapid development in the past decades due to their superior performance  
7 and low unit cost. However, large surface area-to-volume ratio causes serious  
8 adhesive and frictional problems for MEMS operations. Nanotribology is a study  
9 of the interaction between contact surfaces at nanoscale, from chemistry and  
10 physics to material science and mechanical engineering, and is of extreme tech-  
11 nological importance to the application and development of MEMS. This chapter  
12 will attempt to cover the range from preparation of organic thin films to instru-  
13 ments and measurement protocols. We will describe this process in steps. The  
14 preparation of thin film materials (i.e., ionic liquids, multiply-alkylated cyclo-  
15 pentane or self-assembled molecules) and film deposition are presented. Also, the  
16 methods of film evaporation are considered. We examined the relationship of  
17 adhesion and lateral force data to their fundamental aspects at molecular level. The  
18 main objective will be to provide more thorough examination to the interested  
19 reader, and to provide a source to further raise the critical issues concerning the  
20 relationship between surface properties and MEMS application. Fluorinated  
21 molecules with coplanar structure were successfully self-assembled onto silicon  
22 surface. The fluorinated monolayers possessed excellent adhesion-resistance,  
23 friction-reduction and anti-wear durability, which were attributed to low interfacial  
24 energy of end group and dual layer structure of the films. The spatial distribution  
25 of the multi-component film was evaluated by adhesion statistic measurement.  
26 Multialkylated cyclopentanés (MACs) are potential lubricants for space and  
27 MEMS application due to their extreme low volatility. A series of MACs were  
28 synthesized by Dean-Stark trap, autoclave, and phase transfer catalysis methods.  
29 Nanoscale dual-layer films consisting of both MACs and self-assembled mono-  
30 layers (SAMs) were prepared and their morphology, wettability and tribological  
31 properties were investigated. Molecularly thin ILs films with different molecular

---

Y. Mo · L. Wang (✉)

State Key Laboratory of Solid Lubrication, Lanzhou Institute of Chemical Physics,  
Chinese Academy of Sciences, Lanzhou 730000, P. R. China  
e-mail: lpwang@licp.cas.cn

32 structures which showed excellent tribological performance were designed, syn-  
 33 thesized and prepared successfully on silicon surface by dip-coating method. The  
 34 influences of anion, cation and post-treatment on wettability and tribological  
 35 properties of ILs films were investigated systematically. To enhance the wetta-  
 36 bility and to improve the nanotribology of nano films, surface texture technique is  
 37 reviewed. Regular and biomimetic surface textures were fabricated by local anodic  
 38 oxidation (LAO). Dimension of the pillars were precisely controlled by operation  
 39 parameters such as pulse bias voltage, pulse width and humidity. The H-passivated  
 40 Si showed higher growth rate and thicker saturated oxide film than common p- or  
 41 n-type Si under the same oxidation condition. The H-passivated Si employed in  
 42 LAO process can improve lateral resolution of patterns. The adhesive and friction  
 43 force of LAO pattern were measured by AFM colloidal probe. The friction forces  
 44 are closely related to the surface coverage of the nanotexture. The results indicate  
 45 that nanotextures significantly reduced the friction force, while H-passivated Si  
 46 showed large friction force, this is because of the less adhesive energy dissipated  
 47 during sliding on textured surface. The surface nanotextures of biological origins  
 48 were fully duplicated on surface based on duplication method. The morphology  
 49 and the size of the surface textures of the replicas are almost in accordance with  
 50 their biological sources. The wettability of the surfaces was improved with  
 51 hydrophobicity after duplicating with textures. And the biomimetic textures have  
 52 shown to improve nanotribological performance.

## 53 Contents

54	Introduction.....	83
55	Tribological Behavior of Perfluorinated Carboxylic Acid and Hydrogenated	
56	Carboxylic Acid SAMs.....	84
57	Nanotribological Properties of Monolayers Under Ambient Condition:	
58	Effect of Temperature and Humidity.....	87
59	Structural Forces due to Surface Structure: Preparation and Tribological Properties	
60	of Perfluorinated Carboxylic Acid Dual-Layer SAMs.....	89
61	Preparation and Nanotribological Properties of Multi-Component Self-Assembled	
62	Dual-Layer Film.....	90
63	Tribological Behavior of Multiply-Alkylated Cyclopentane.....	92
64	Effect of Wettability on Nanotribology of MACs.....	93
65	Distribution and Positioning of Lubricant on a Surface Using the Local Anodic	
66	Oxide Method.....	93
67	Tribological Behavior of Ionic Liquid Films.....	97
68	Effect of Anion and Substrate Modification.....	98
69	Effect of Bonding Percentage and Alkyl Chain Length.....	98
70	Effect of Function Group and Annealing Treatment.....	101
71	IL Films with Dual-Layer Structure.....	102
72	Enhancement of Nanotribology and Wettability by Surface Textures	
73	in Adhesion Resistant.....	104
74	Regular Surface Textures.....	104
75	Biomimetic Surface Textures.....	106
76	Summary and Outlook.....	108
77	References.....	109

79  
78

## Introduction

80 The microelectromechanical systems (MEMS) have received rapid development in  
81 the past decades due to their superior performance and low unit cost. However,  
82 large surface area-to-volume ratio causes serious adhesion and frictional problems  
83 for MEMS operations. In MEMS devices, various forces associated with the  
84 device scale down with the size. When the length of the machine decreases from  
85 1 mm to 1  $\mu\text{m}$ , the area decrease by a factor of million and volume decreases by a  
86 factor of a billion. At this scale, mechanical loading is often not the overwhelming  
87 force as in macroscale, and surface forces such as van der Waals, electronic and  
88 capillary force that are proportional to area, become a thousand times larger than  
89 the forces proportional to volume. In addition to the consequence of a large area-  
90 to-volume ratio since MEMS devices are designed for small tolerance, physical  
91 contact becomes more likely, which makes them particularly vulnerable to  
92 adhesion between adjacent components. Slight particulate or chemical contami-  
93 nation present at the interface can lead to failure. Since the start up forces and  
94 torques involved in operation available to overcome retarding forces are small in  
95 MEMS, the increase in resistive forces such as adhesion force and lateral friction  
96 force become a serious tribological concern that limits the durability and reliability  
97 in MEMS. A large friction force is required to initiate relative motion between two  
98 surfaces, that is large static friction, which has been thoroughly studied in the field  
99 of data magnetic storage. The adhesion is generally measured by the amount of  
100 force necessary to separate two surfaces in contact. Adhesion, friction, wear can  
101 affect MEMS performance and even lead to failure.

102 Space lubrication and nanotechnology are driven by the trends such as device  
103 miniaturization, better integrated functional components and energy saving  
104 properties. MEMS as miniaturized devices are operated under very narrow space  
105 and small normal load. They cannot be lubricated with lubrication oils, but usually  
106 employ thin films whose thickness is well below a few nanometers. The adhesive  
107 force comes largely from meniscus force and viscous force, rather than the applied  
108 loads. The perfluoropolyether (PFPE) thin films are the most widely used lubri-  
109 cants in data storage devices, but PFPEs usually experience metal catalytic deg-  
110 radation and are normally expensive. The potential of self-assembled monolayers  
111 (SAMs), multiplyalkylated cyclopentanes (MACs) and ionic liquids (ILs) as thin  
112 lubricant films were exploited by a number of researchers aiming to replace  
113 PFPEs. The molecular structure, length of alkyl chains, functional groups, surface  
114 microstructure and substrate modification are key factors which affect the wetta-  
115 bility and the nanotribological behavior of these thin films.



## 116 Tribological Behavior of Perfluorinated Carboxylic Acid 117 and Hydrogenated Carboxylic Acid SAMs

118 Molecular thin films of several monolayers or less supported by surfaces exhibit  
119 considerable departure from bulk behavior, which is mainly due to molecular  
120 alignment or ordering. SAMs have been widely investigated during the past  
121 decade because of their potential applications in the field of surface modification,  
122 boundary lubricant, sensor, photoelectronics, and functional bio-membrane mod-  
123 eling etc. On the basis of the synthetic approaches and the surface chemical  
124 reactions, the chemical structures of SAMs can be altered easily both at the  
125 individual molecular and at the material levels. The nanotribological properties of  
126 SAMs, which are potential lubricants for controlling adhesion and friction, are  
127 closely related to their intrinsic chemical composition and structure. For example  
128 the friction behaviors of SAMs are terminal group and chain length dependent.  
129 SAMs with long chains are generally densely packed, while the shorter chain ones  
130 are not. With the same terminal group, loosely packed SAMs generally possess  
131 higher friction force due to the large energy dissipation during the relative  
132 movement, and adhesive force as well due to the liquid-like disordered structure.  
133 On the other hand, altering the terminal group, from apolar to polar, could result in  
134 the increase of adhesion and friction. This is because SAMs with more relatively  
135 strong interaction during the relative movement, and therefore higher adhesion and  
136 more energy loss are expected, which leads to a higher friction force. Mix-  
137 deposition of molecules with different terminal group or alkyl chain lengths to  
138 form mixed SAMs is also extensively studied, which allows an understanding of  
139 the relationship between structure and performance of SAMs in wide and depth.

140 As an example of tribological behavior of perfluorinated and hydrogenated  
141 carboxylic acid (FC and HC) SAMs on aluminum surface by chemical vapor  
142 deposition were studied [1]. Figure 3.1 shows the mechanism of adsorption of  
143 SAMs. The samples were placed in a 100 ml sealed vessel with a glass container  
144 filled with 0.2 ml FC or HC precursor. There was no direct contact between the  
145 samples and precursor. The vessel was placed in an oven and then nitrogen gas  
146 was filled in the oven. The samples were annealed in nitrogen at 200 °C for 3 h,  
147 and then cooled in a desiccator. The precursor vaporized and reacted with substrate  
148 surface on each sample, resulting in the formation of SAM. Then, the samples  
149 were rinsed with chloroform, acetone, ethanol, and deionised water successively to  
150 remove other physisorbed ions and molecules. The deposition of SAMs relied on  
151 the chemisorption of reactive head groups presented in the adsorbate molecules on  
152 the substrate surface in order to anchor them.

153 X-ray photoelectron spectroscopy (XPS) was used to evaluate the relative  
154 atomic composition on the surface of SAMs. The procedure involved the mea-  
155 surement of the Al2p, F1s and C1s core level spectra for surfaces of these films.  
156 The data of Al2p features from bare surface are shown in Fig. 3.2a and are  
157 associated with Al<sub>2</sub>O<sub>3</sub> or AlO(OH) (74.7 eV) and Al (72.7 eV). This result indi-  
158 cates that the outmost layer of Al is converted to aluminum oxide under ambient

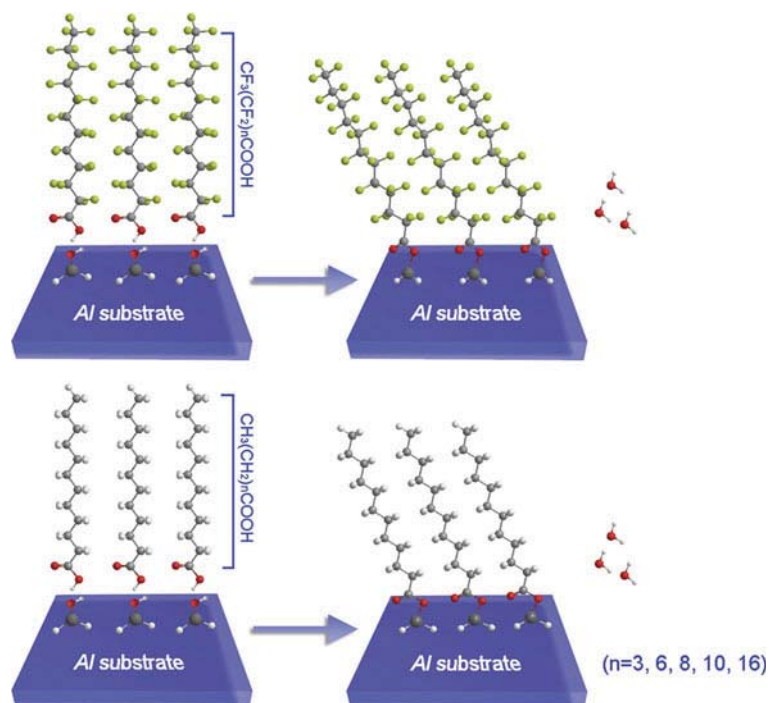


**Fig. 3.1** Schematic structure and forming process of perfluorinated carboxylic acid and hydrogenated carboxylic acid molecules chemically adsorbed onto aluminum substrate. Perfluorinated carboxylic acid and hydrogenated carboxylic acid SAMs are of similar chain length and head group monolayers with different backbone groups. Reproduced with permission from Ref. [1]. Copyright (2009) Surface and Interface analysis

159 condition. A single F1s feature resulting from FC18 adsorption on aluminum oxide  
 160 is shown in Fig. 3.2b. The F1s feature at 688.7 eV is assigned to  $-\text{CF}_2-$  and  $-\text{CF}_3$   
 161 groups, which indicates the fluorine element on the substrate surface. Figure 3.2c  
 162 displays the C1s spectra obtained from one set of FC SAMs with various chain  
 163 lengths (C5–C18) on aluminum oxide surface. The C1s features are assigned to  
 164  $-\text{CF}_3$  group ( $\sim 293.5$  eV),  $-\text{CF}_2-$  group (C5: 292.1–C18: 291.5 eV) [2, 3], car-  
 165 boxylate group ( $\text{COO}^-$ , 289.2 eV), [4] and a feature (284.8 eV) associated with  
 166 adventitious carbon possibly from airborne hydrocarbon contamination. It is  
 167 suggested that the samples were strongly bonded with airborne organics (fatty  
 168 acid, etc.), which were adsorbed at film defects and imperfections and were not  
 169 easily removed by vacuum pumping. It is also observed that the intensity of  
 170 adventitious carbon decreased rapidly with increase of fluorocarbon chain length  
 171 while that of  $\text{COO}^-$  and  $-\text{CF}_3$  remained constant. This is because the long chain  
 172 FC-SAMs were densely packed and with fewer defects, which prevented airborne  
 173 organics from adsorbing onto the film. Figure 3.2d shows a similar tendency of  
 174 increase in C concentration associated with the increase of chain length in

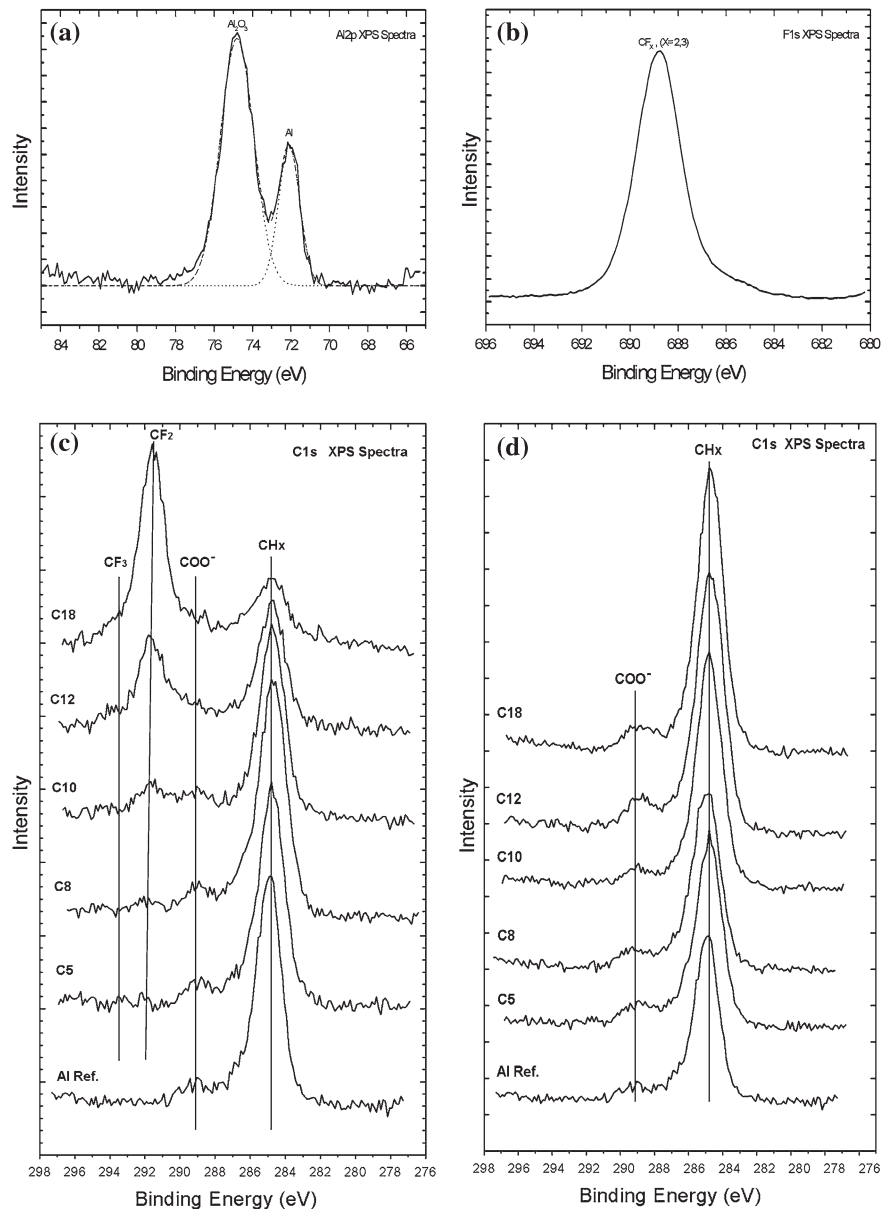


**Fig. 3.2** XPS spectra of Al 2p **a** F 1s, **b** C1s, **c** region of the FC5-FC18 SAMs, **d** C 1s region of the HC5-HC18 SAMs. Reproduced with permission from Ref. [1]. Copyright (2009) Surface and Interface analysis



Editor Proof

175 HC-SAMs. In addition, two features arose from C1s, as shown in this figure, the  
 176 left feature assigned to carboxylate group (COO, 289.2 eV) and the right feature  
 177 can be attributed to CHx (284.8 eV).

178 ***Nanotribological Properties of Monolayers Under Ambient***  
 179 ***Condition: Effect of Temperature and Humidity***

180 The adhesive force between AFM tip and SAM surfaces under various relative  
 181 humidity are shown in Fig. 3.3a and b. The bare aluminum surface showed higher  
 182 adhesive force than SAMs deposited on it. Between FC and HC SAMs, the FC-  
 183 SAMs showed lower adhesion force than HC-SAMs with same chain length,  
 184 which indicates that adhesive force is consistent with the difference in surface  
 185 energy ( $15 \text{ mJ/m}^2$  for  $\text{CF}_3$ -terminated compared to  $19 \text{ mJ/m}^2$  for  $\text{CH}_3$ -terminated  
 186 SAMs [5]). The relationship between adhesive forces for bare Al and FC-SAMs  
 187 with various chain lengths is shown in Fig. 3.3a. It shows that adhesive force

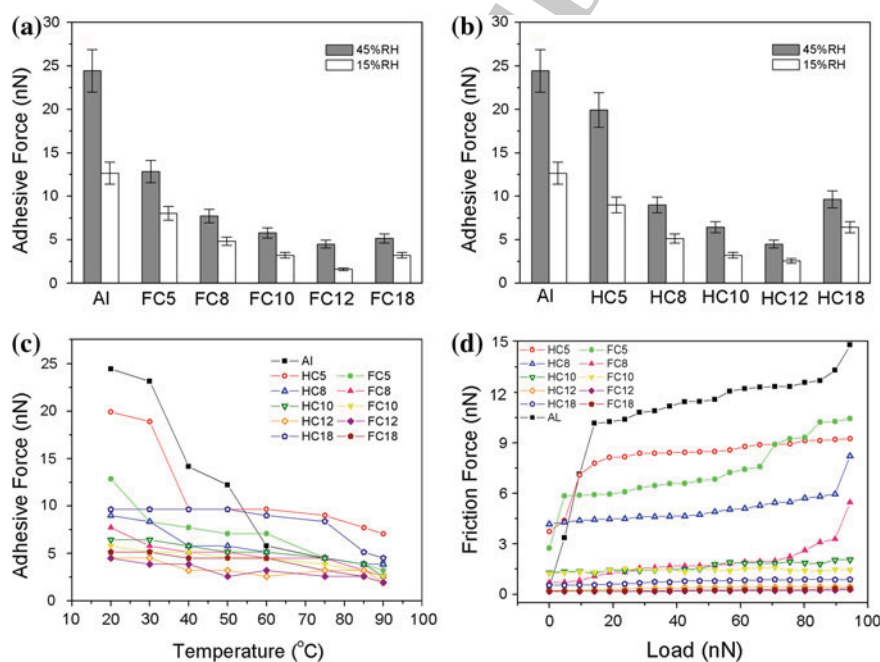


**Fig. 3.3** Relative humidity dependence of adhesion for Al substrate and various SAMs. **a** FC-SAMs. **b** HC-SAMs. **c** Dependence on temperature of adhesion for the Al substrate, FC-SAMs (*solid symbols*) and HC-SAMs (*empty symbols*). **d** Plots of friction force versus load, for various SAMs on Al substrate, FC-SAMs and HC-SAMs. Reproduced with permission from Ref. [1]. Copyright (2009) Surface and Interface analysis



188 increased with relative humidity (RH), which is due to water menisci contribution.  
189 It is also observed that the adhesive force of FC-SAMs with chain lengths up to ten  
190 carbons increased indistinctively and then tended to a stable value. This tendency  
191 of the adhesive force agrees well with the change in contact angles which corre-  
192 lates with surface energy [1]. FC12 and FC18 SAMs showed lowest adhesive  
193 forces and highest contact angles, which implies that 12-carbon and 18-carbon  
194 chains are prone to form more stiff film. In the case of short chain SAMs (n-carbon  
195 <10), they formed relatively soft monolayers and tended to disorder under the  
196 pressure applied by AFM tip. The pressure induced terminal defects may be  
197 sufficient for complete disorder, an effect that will be magnified by the reduced  
198 packing density of the short molecules. For SAMs with chain lengths up to ten  
199 carbons, low adhesive force may be attributed to high stiffness, which gives rise to  
200 a smaller contact area for the same applied load. Figure 3.3c shows the influence  
201 of temperature on adhesion. The adhesive force decreased with increase of tem-  
202 perature and then tended to a stable value. The drop in adhesive force is a result of  
203 desorption of water molecules and the corresponding decrease of water menisci  
204 contribution. The aluminum substrate and short chain SAMs showed more tem-  
205 perature dependence compared with long chain SAMs. The FC and HC SAMs  
206 with long chains exhibit temperature independence over the temperature range  
207 studied, which is due to the fact that highly hydrophobic nature of these mono-  
208 layers results in less formation of water menisci. It indicates that long backbone  
209 chains and neighboring fluorine atoms provide stronger inter-chain interaction  
210 compared to that provided by short backbone chain and hydrogen atoms. SAMs  
211 with perfluorinated long chains were densely packed and highly ordered with  
212 solid-state-like properties at high temperature due to strong inter-chain van der  
213 Waals force.

214 Figure 3.3d shows the relationship between friction force and external load for  
215 bare Al, as well as for FC and HC SAMs with various chain lengths, at RH of  
216 15 % and temperature of 20 °C. The bare aluminum surface without organic film  
217 generates the highest friction. This may be attributed to the highest surface energy  
218 on the Al<sub>2</sub>O<sub>3</sub>-covered surface. The highest surface energy can be indicated by the  
219 lowest contact angle. It is a general tendency that the friction force decreases as  
220 chain length increases and FC-SAMs showed lower friction force than HC-SAMs  
221 of corresponding chain length. It is also observed that the friction properties of  
222 SAMs do not depend only on the chemical nature of terminal groups. Otherwise,  
223 all chain lengths should yield similar friction values. For the formation of SAMs,  
224 both surface energy and Inter-chain interactions play important roles and deter-  
225 mine quality and character of the SAMs [6]. The decrease of friction is mainly due  
226 to SAMs with longer chain, as they generally possess relatively stronger inter-  
227 chain interaction, which give rise to a smaller contact area for the same applied  
228 load during the sliding. Tribological characterization studies of the SAMs can be  
229 summarized as shown in Table 3.1 [1].

**Table 3.1** Summary of tribological properties for the FC arid HC SAMs on Al surface

	SAMs property	Adhesive force	Nanofriction	Microfriction
Backbone style	Fluorocarbon backbone	Low	Low	High
	Hydrocarbon backbone	High	High	Low
Chain length	Short ( $Q < 10$ )	High	High	–
	Middle ( $C_n = 10-12$ )	Low	Low	–
	Long ( $C_n > 12$ )	Low	Low	–
Terminal group	Methyl	High	High	Low
	Perfluorinated methyl	Low	Low	High

230 ***Structural Forces due to Surface Structure: Preparation***  
 231 ***and Tribological Properties of Perfluorinated Carboxylic***  
 232 ***Acid Dual-Layer SAMs***

233 SAMs have good anti-rupture properties due to their strong bonding to the sub-  
 234 strate surface, and they are expected not to freely migrate on the surface. However,  
 235 some molecules from SAMs may transfer to the surface of counterpart when  
 236 external force was applied on the contacting surface [7]. Because of monolayer  
 237 structure and flexibility, SAMs exhibit poor anti-wear durability [8–10]. To utilize  
 238 SAMs as lubricants to protect MEMS, it is necessary to consider the molecule  
 239 layer structure as well as the strongly bonded characteristics of lubricant [11].  
 240 Generally, there are two approaches to obtain these more complex structures on  
 241 surface: one is to synthesize target precursors with functional groups and then  
 242 assemble them onto surfaces by a one-step method, [12–17] but there are diffi-  
 243 culties in purification during the synthesis of more complex molecules. Another is  
 244 stepwise formation of the film with desired structures based on surface chemical  
 245 reaction.

246 Several reports [13–15] have demonstrated that incorporation of amides into  
 247 hydrocarbon backbones of precursor could improve the stability of SAMs. The  
 248 reason was that the amide underlayers were capable of being cross-linked by  
 249 hydrogen bonding. Work has also recently been done on building amide-con-  
 250 taining dual layer SAMs on silicon surfaces and found to be very excellent wear-  
 251 resistant films [16, 17]. Bai et al. [18] designed a perfluorinated dual layer structure  
 252 which can help to improve the film quality, reduce the friction and significantly  
 253 enhance their durability, as shown in Fig. 3.4.

254 A self-assembled dual-layer film was prepared on single-crystal silicon surface  
 255 by chemisorption of perfluorododecanoic acid (PFDA) molecules on 3-amino-  
 256 propyltriethoxysilane (APS) SAM with terminal amino group. The dual-layer  
 257 PFDA–APS film was hydrophobic with the contact angle for water to be about  
 258  $105^\circ$  and the overall thickness about 2.5 nm. Atomic force microscopic images  
 259 revealed that the APS surface was initially characterized with uncontinuous  
 260 asperities, the surface became relatively smooth and homogeneous after coating  
 261 with PFDA film by self-assembly. The PFDA–APS film exhibited low

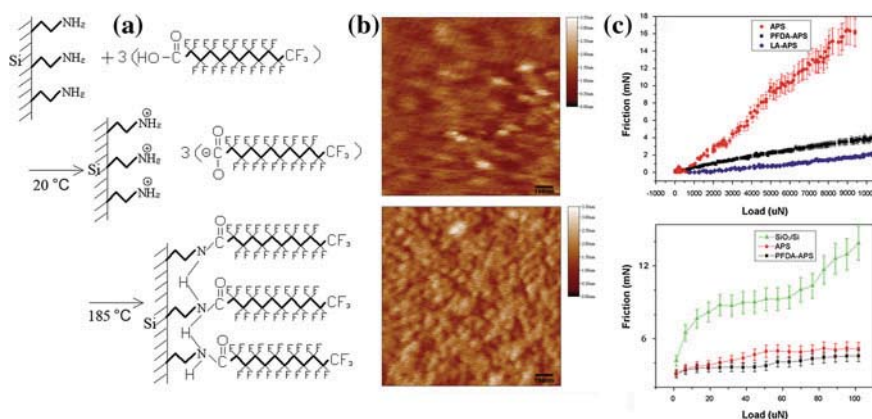


**Fig. 3.4** **a** Schematic structure and forming process of PFDA molecules chemically adsorbing onto APS monolayer surface. **b** AFM topographic images of APS monolayer and PFDA-APS dual-layer film on silicon wafer. **c** Microtribological behaviors of the APS monolayer, PFDA-APS dual-layer film and LA-APS dual-layer film surfaces sliding against a steel ball. Reproduced with permission from Ref. [18]. Copyright (2008) Journal of Physical Chemistry C

262 adhesion and it greatly reduced the friction force at both nano- and microscale. The  
 263 film exhibited better anti-wear durability than the lauric acid (dodecanoic acid or  
 264 LA)-APS self-assembled dual-layer film with same chain length and similar  
 265 structure.

### 266 *Preparation and Nanotribological Properties of Multi-* 267 *Component Self-Assembled Dual-Layer Film*

268 Previous results [18–20] indicate that the dual-layer structure can help to improve  
 269 the film quality and enhance their durability and load bearing capacity. Mean-  
 270 while, it is observed that a hydrogenated carboxylic acid dual-layer film exhibits  
 271 better friction reduction but poorer durability compared to the perfluorinated  
 272 carboxylic acids dual layer. A lubrication system consisting of dual component  
 273 self-assembled dual-layer films was designed to minimize friction and a molecular  
 274 mixture layer to prolong durability. Bai's group [21] reported a novel strategy for a  
 275 dual-component self-assembled film with control of spatial growth on a large  
 276 surface area based on a dip-coating nanoparticles method. In selecting among the  
 277 various SAMs, we particularly focus on the control of both fluorinated and  
 278 hydrogenated backbone chain molecules because these molecules have strong  
 279 potential applications in MEMS.

280 The mechanism of this site-selective growth can be explained as follows. An  
 281 APS layer was first formed on hydroxylated silicon substrate. Monodisperse Ag

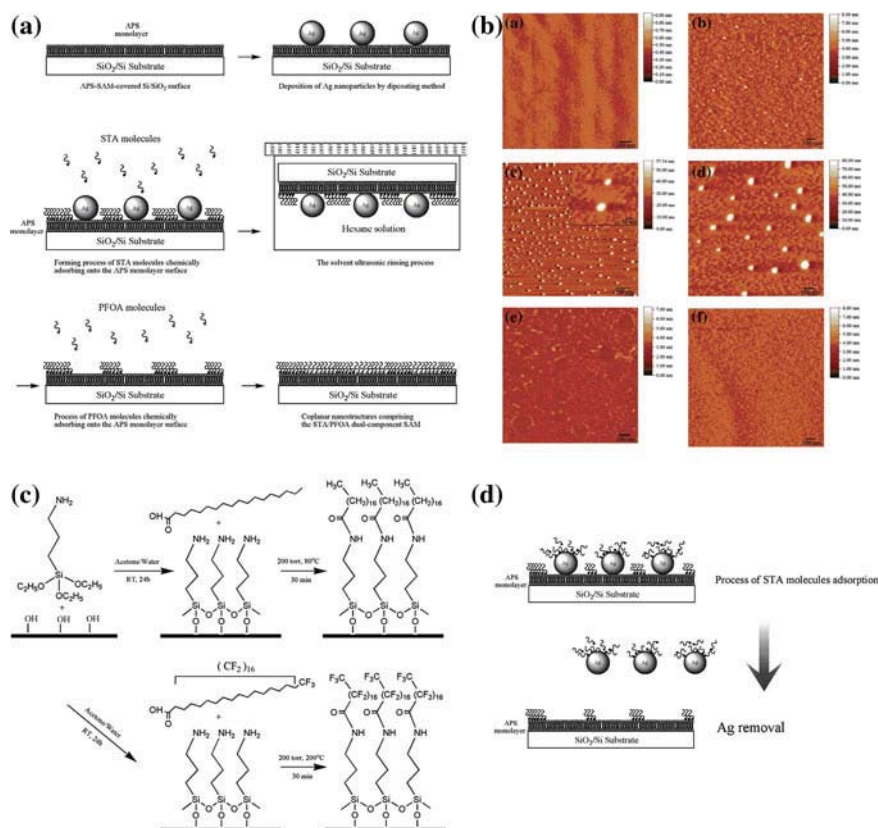
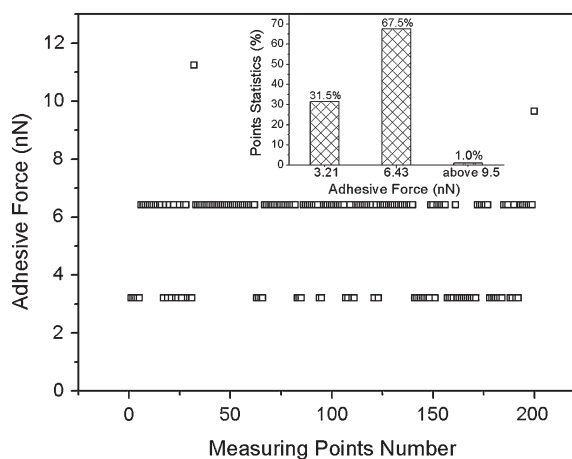


**Fig. 3.5** **a** Formation of the coplanar nanostructure STA/PFOA dual-component dual-layer film; **b** AFM images of the film surface in each step; **c** Chemical structure and forming process of STA and PFOA molecules chemically adsorbing onto the APS monolayer surface; **d** Mechanism of STA molecules deposition and Ag nanoparticles removal. Reproduced with permission from Ref. [21]. Copyright (2008) Journal of Physical Chemistry C

282 nanoparticles capped by long-chain carboxylates played a role in the effective  
 283 suppression of undesired composite growth on sites. Due to acid amide reaction  
 284 between stearic acid (STA) and APS molecules, the STA molecules chemisorbed  
 285 onto the APS-modified surface. The film surface fabricated lunar crater-like pits  
 286 microstructure and amino-terminated surface exposed in the bottom of the pits  
 287 after Ag nanoparticles removal. The perfluorooctadecanoic acid (PFOA) mole-  
 288 cules absorbed onto the exposed amino terminated surface with acid amide  
 289 reaction, and the pits of the film were occupied completely by PFOA molecules  
 290 (Fig. 3.5).

291 It is important to calculate the spatial distribution of the dual-component film by  
 292 adhesion statistic measurement, as shown in Fig. 3.6. Adhesive forces of STA and  
 293 PFOA SAMs were measured as 3.21 and 6.43 nN, respectively. The adhesive

**Fig. 3.6** Plot of adhesion force and statistical distribution for the PFOA/STA-APS film (20 °C, 15 % RH). Reproduced with permission from Ref. [21]. Copyright (2008) Journal of Physical Chemistry C



294 force measurement was typically performed at a rate of 1 Hz along the scan axis  
 295 and a scan size of  $10 \times 10 \mu\text{m}$  during scanning, at least 200 measuring points  
 296 were carried out for each scan range. From the inset, it can be seen that the  
 297 adhesive forces of the dual-component layer were calculated statistically as 31.5  
 298 and 67.5 %, respectively. The surface coverage of the pits was calculated as a  
 299 value of about 20 %, which approaches to surface coverage of the pits calculated  
 300 from the data from the adhesive force measurement. The discrepancy between the  
 301 surface coverage of pits and the statistical value of PFOA in the adhesion mea-  
 302 surement is probably because some STA molecules comprising a SAM exchanged  
 303 gradually when exposed to the PFOA atmosphere, which results from displace-  
 304 ment of SAMs by exchange [22, 23].

### 305 Tribological Behavior of Multiply-Alkylated Cyclopentane

306 To utilize SAMs as boundary lubricants, it is necessary to consider the mobile  
 307 characteristics in addition to the strongly bonded characteristics. The chemically  
 308 bonded SAMs protect the devices during processing and the early stages of use,  
 309 while a mobile lubricant is present to replenish the lubricant coating as the SAMs  
 310 fail. As a result, an ideal boundary lubricant system is pursued.

311 Multiply-alkylated cyclopentanes (MACs) are composed of one cyclopentane  
 312 ring with two to five alkyl groups substituted on the ring. They are synthesized by  
 313 reacting dicyclopentadiene with alcohols of various chain lengths producing a  
 314 lubricant with a selectable range of physical properties [24]. MAC has excellent  
 315 viscosity properties, thermal stability and low volatility for use as lubricant and is  
 316 presently gaining wide acceptance in certain space application [25, 26].



317 ***Effect of Wettability on Nanotribology of MACs***

318 Wettability is one of the most important properties of solid surfaces and has  
319 attracted much attention since the time of Young in 1805 [27]. It is governed by  
320 both chemical composition and topological characteristic of the surface. Con-  
321 trolling wettability is quite important in the study of nanotribological properties.

322 Wang et al. [28] studied wettability of MACs on silicon substrates that were  
323 treated by different cleaning and etching processes. As shown in Fig. 3.7, the  
324 wettabilities of MACs on hydroxylated silicon and hydrogenated silicon are better  
325 than the wettability on bare silicon without pretreatment, and that outcome is  
326 mainly caused by topological structure changes of the surface.

327 Ma et al. [29] investigated wettability and loading-carrying capacity of MACs  
328 on two types of SAMs of decyltrichlorosilane (DTS) and 1H,1H,2H,2H perfluoro-  
329 rodecyltrichlorosilane (FDTS). As shown in Fig. 3.8, when MAC was deposited  
330 on the DTS-SAM, unlike uniform DTS-SAM, the MAC forms as island-like liquid  
331 droplet with a typical diameter of 25 nm and an average height of 3.5 nm was  
332 evenly distributed on the DTS-SAM to form dual-layer film with a surface cover-  
333 age of about 70 %. This research indicate that MAC was deposited on the two  
334 SAMs to form dual-layer films with total thickness of 5 nm, the mobile lubricant  
335 could markedly decrease friction of DTS-SAM and remarkably promote the load-  
336 carrying capacity and durability of both DTS and FDTS SAMs owing to its good  
337 self-repairing property.

338 ***Distribution and Positioning of Lubricant on a Surface***  
339 ***Using the Local Anodic Oxide Method***

340 Local anodic oxidation (LAO) via the atomic force microscope (AFM) is a  
341 lithography technique perspective for the fabrication of nanometer-scaled struc-  
342 tures and devices. AFM-LAO is based on direct oxidation of the sample by  
343 negative voltage applied to the AFM tip with respect to the surface of the sample.  
344 The driving force is the faradaic current flows between the tip and sample surface  
345 with the aid of the water meniscus. When the faradaic current flows into water  
346 bridge, H<sub>2</sub>O molecules are decomposed into oxyanions (OH<sup>-</sup> and O<sup>-</sup>) and protons  
347 (H<sup>+</sup>). These ions penetrate into the oxide layer because of the high electric field  
348 ( $E > 107$  V/m), [30] leading to the formation and subsequent growth of SiO<sub>2</sub> on  
349 the H-passivated Si surface. The AFM-LAO process can be used not only in  
350 fabrication of nanodevices but also in adhesion resistance and friction reduction as  
351 in the case of surface texturing. In previous studies [31, 32], AFM-LAO has been  
352 demonstrated to be the most promising tool for fabricating nanodots and lines on  
353 several types of materials ranging from metals to semiconductors. The LAO  
354 process is controlled by several major parameters as follows: pulsed bias voltage,  
355 pulsewidth and humidity, as shown in Fig. 3.9.

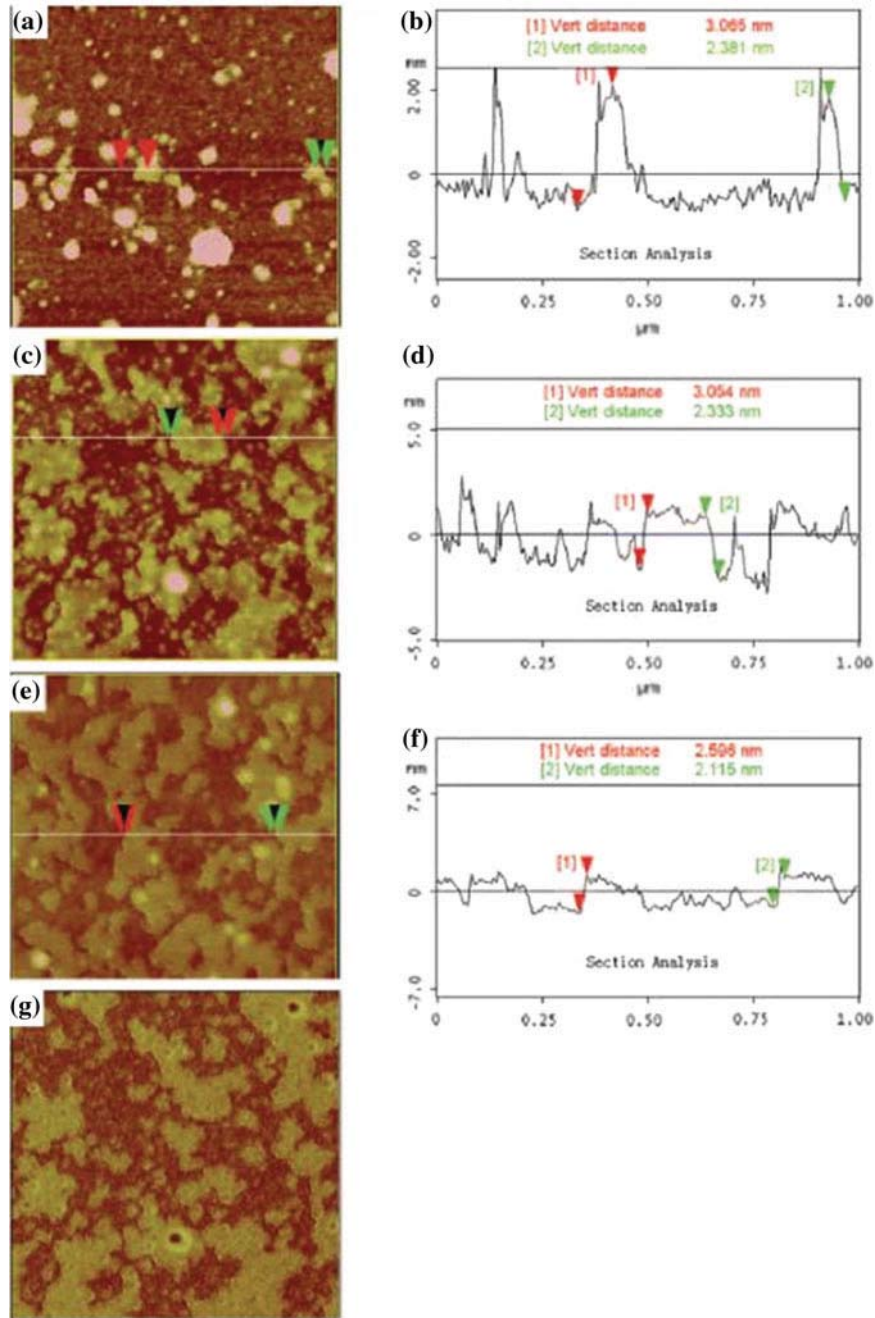


**Fig. 3.7** AFM images of MACs films: **a** MACs on bare silicon; **b** line section analysis of (**a**); **c** MACs on hydroxylated silicon; **d** line section analysis of (**c**); **e** MACs on hydrogenated silicon; **f** line section analysis of (**e**); **g** phase map for (**c**). Reproduced with permission from Ref. [28]. Copyright (2010) Tribology Transactions



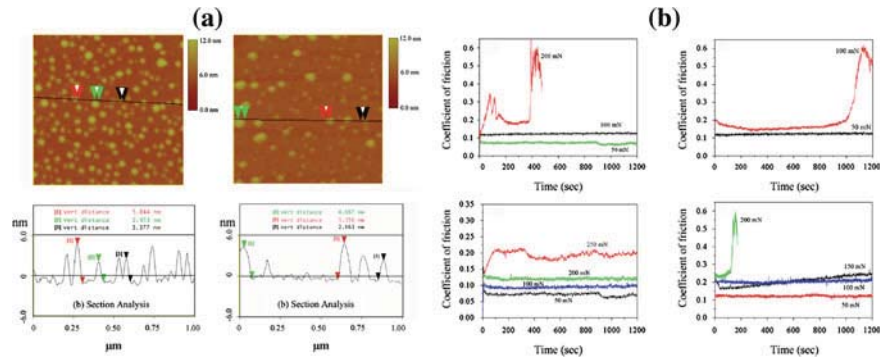


**Fig. 3.8** **a** AFM images and section analysis of MAC-DTS dual-layer; **b** friction coefficient and durability of designed SAMs. Reproduced with permission from Ref. [29]. Copyright (2007) Elsevier B. V

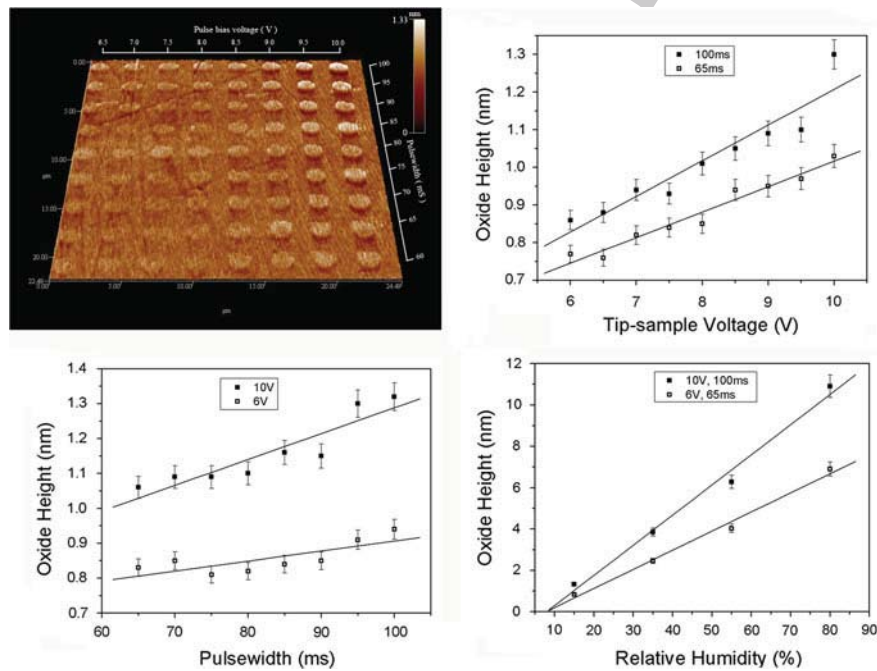


**Fig. 3.9** A testing array of Si pillars prepared at different operation parameters, and the oxide height as a function of tip-sample pulse bias voltage, pulsewidth and relative humidity, respectively. Reproduced with permission from Ref. [32]. Copyright (2008) Elsevier B. V

356 As above mentioned, MAC has excellent viscosity properties, thermal stability,  
 357 and low volatility for use as a lubricant. Unfortunately, it is difficult to control the  
 358 size and distribution of lubricants precisely on silicon or DLC. Currently, Bai et al.

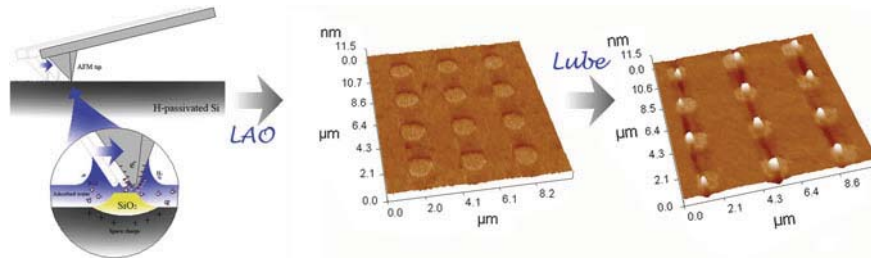


**Fig. 3.10** Schematic of distribution and positioning process of MAC on a surface using the local anodic oxide (LAO) method. Reproduced with permission from Ref. [33]. Copyright (2009) Langmuir

359 [33] utilizes an AFM-LAO technique to control the size and distribution of  
 360 lubricants precisely in an atmospheric environment. The new technique includes  
 361 two main steps: the production of nanometer-sized nanopatterns using AFM-LAO,  
 362 followed by the selective adsorption of MAC lubricant onto these patterns using  
 363 dip-coating method (Figure 3.10).

364 Ducker [34] first introduced the use of colloidal probe tips by attaching a sphere  
 365 to the cantilever to measure adhesion. The spherical shape of the tip provides  
 366 controlled contact pressure, symmetry, and mostly elastic contacts. For adhesion  
 367 and friction force measurements of the fabricated MAC matrix, the spherical probe  
 368 tip can fully contact with surface, while sharp tip can only have point contact.

369 The adhesive force between the colloidal probe and sample surfaces is shown in  
 370 Fig. 3.11a. A strong adhesive force was observed on the untreated H-passivated  
 371 silicon surface, on which the adhesive force was about 175 nN. After the patterns  
 372 were generated, the adhesive force was decreased to 70 nN. This result indicates  
 373 that the pattern exhibited adhesion resistance. Adhesion is directly related to the  
 374 bearing ratio, which describes the real area of contact between two solid surfaces.  
 375 After dip-coating in MAC solution, the adhesive forces of untreated H-passivated

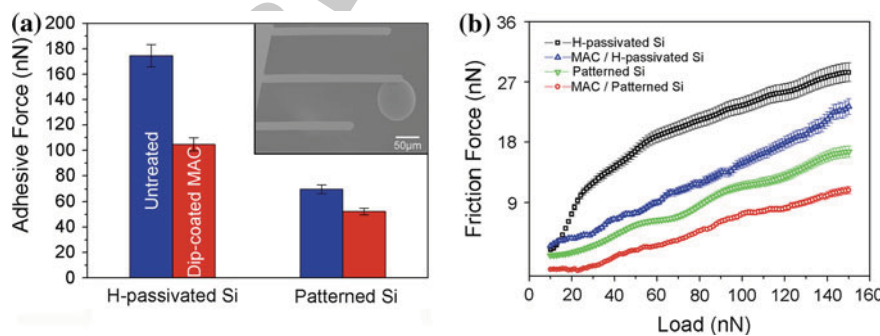


**Fig. 3.11** Plots of **a** adhesive forces and **b** friction force between the AFM colloidal probe and the surfaces of samples. The inset shows an SEM image of a typical colloidal probe. Reproduced with permission from Ref. [33]. Copyright (2009) Langmuir

376 and patterned Si were decreased to 105 and 52 nN, respectively. Such a phe-  
377 nomenon indicates that the MAC layer on the sample surface can obviously lower  
378 the interfacial energy and capillarity between the tip and surface. Figure 3.11b  
379 presents the plot of friction versus load curves for the bare H-passivated Si and  
380 patterned Si and these surfaces treated with MAC. Patterned Si evidently reduced  
381 the friction force, and the MAC-cover-patterned Si exhibited the lowest friction  
382 force whereas H-passivated Si had a strong friction force. The decrease in friction  
383 force is mainly due to a pattern giving rise to a smaller contact area for the same  
384 applied load and MAC as the lubricant layer minimizes the shearing strength  
385 during sliding.

### 386 Tribological Behavior of Ionic Liquid Films

387 Why can ILs be lubricants? ILs have many unique properties, such as negligible  
388 volatility at a relatively high temperature, nonflammability, high thermal stability,  
389 etc. [35]. These characteristics have attracted great attention and made them  
390 available in many potential applications, for example catalysis, electrochemistry,  
391 separation science for extraction of heavy metal ions, as solvents for green  
392 chemistry, and materials for optoelectronic applications [36–39]. On the other  
393 hand, as is well known to tribologists, these characteristics are also just what high  
394 performance lubricants demand. Very harsh friction conditions require lubricating  
395 oils to have high thermal stability and chemical inertness. The decomposition  
396 temperatures of imidazolium ILs are generally above 350 °C, some even as high as  
397 480°C, together with the low temperature fluidity (the glass transition temperature,  
398  $T_g$  below 50°C, even 100°C) means that ILs can function in a wide temperature  
399 range. In addition, low volatility makes ILs applicable under vacuum, especially  
400 for spacecraft application. The above mentioned properties of ILs also make them  
401 excellent lubricants. Ye et al. [40, 41] investigated the tribological behavior of two  
402 kinds of alkylimidazolium tetrafluoroborate and found them versatile lubricants for  
403 the contacts of steel/steel, steel/aluminum, steel/copper, steel/SiO<sub>2</sub>, Si<sub>3</sub>N<sub>4</sub>/SiO<sub>2</sub>,  
404 steel/Si (100), and steel/sialon ceramics.

405 Different with large scale mechanical system, MEMS cannot be lubricated with  
406 lubrication oils, but can use a thin lubrication film whose thickness is well below a  
407 few tens of nanometers. The viscous force comes largely from the viscosity of  
408 lubricant films and the meniscus force, rather than the applied loads; this dictates  
409 the extent of friction and the mechanisms of lubrication failure. The PFPEs of  
410 nanometer thickness are the most widely used lubricants in miniaturized devices,  
411 but usually experience metal catalytic degradation and are normally expensive.  
412 The potential of ILs in thin film lubrication was exploited by a number of  
413 researchers aiming to replace PFPEs [42–46]. The molecular structure, the counter  
414 anion, the length of substituted alkyl chains and the functional groups, have key  
415 effects on the adhesion and tribological behavior of IL films. The interaction



416 between lubricant and surface cannot only determine the wetting of lubricant but  
417 also determine its durability [47].

### 418 *Effect of Anion and Substrate Modification*

419 The anions have a more complicated effect on tribological properties in that they  
420 cannot only change the viscosity but also surface energy. For ILs with same  
421 cations, Zhu et al. [48] demonstrated three kinds of 3-butyl-1-methyl imidazolium  
422 ILs with anions of hexafluorophosphate, tetrafluoroborate and adipate as ultra-thin  
423 film. Mo et al. [49] introduced a series of propylmethylimidazolium (PMIM) base  
424 wear resistant ionic liquid with anions of bromide, carbonate, chloride and sulfite.  
425 Adhesion and friction measurements at nanoscale were carried out using a col-  
426 loidal probe. As shown in Fig. 3.12, based on topography analysis, IL films are  
427 found to be prone to attach to the silicon substrate surface, leading to more uniform  
428 thin films. Bromide and sulfite anions show favorable lubrication as seen from  
429 adhesion and friction, which are less than those of carbonate, chloride and  
430 uncoated silicon. The wear test of the IL films was evaluated at loads ranging from  
431 60 to 300 mN and sliding frequency in range 1–20 Hz. IL films showed favorable  
432 friction reduction and durability. Imidazolium with anions of chloride and  
433 carbonate exhibited a low friction coefficient at a normal load of 200 mN. Imi-  
434 dazolium sulfite exhibits low friction and anti-wear durability even at high-  
435 frequency sliding (20 Hz).

### 436 *Effect of Bonding Percentage and Alkyl Chain Length*

437 The lubricant adsorbed onto silicon after the solvent rinsing process, which is  
438 termed as bonding lubricant. The bonding percentages of ionic liquid were mea-  
439 sured in terms of the thickness of ionic liquid adsorbed onto silicon surface  
440 [%bonding =  $100 \times (\text{final film thickness}/\text{initial film thickness})$ ]. Sinha et al. [50]  
441 have also used the similar definition while computing the bonded ratio. To  
442 understand the influence of the ratio of bonding to the mobile fraction on the  
443 friction in microscale behavior, the mixed IL films were compared with different  
444 ratios of bonding to mobile fraction to understand the effect of different bonding  
445 percentages. Mo et al. [44] prepared the four kinds of samples (viz. 0, 15, 60 and  
446 85 %) by controlling self-assembled conditions. Fig. 3.13a–e shows the friction  
447 coefficients and sliding cycles of 1-alkyl-3-ethylcarboxylic acid imidazolium  
448 chloride (AEImi-Cl) ionic liquid with various bonding percentages, as a function  
449 of sliding cycles against a steel ball at normal loads ranging between 60 and  
450 500 mN and a sliding velocity of 10 mm/s. Figure 3.13 shows the IL films  
451 bonding percentage of 0, 15, 60, and 85 % at a normal load of 60 mN, an average  
452 friction coefficient of 0.28, 0.22, 0.18, and 0.16 was recorded, respectively. It was

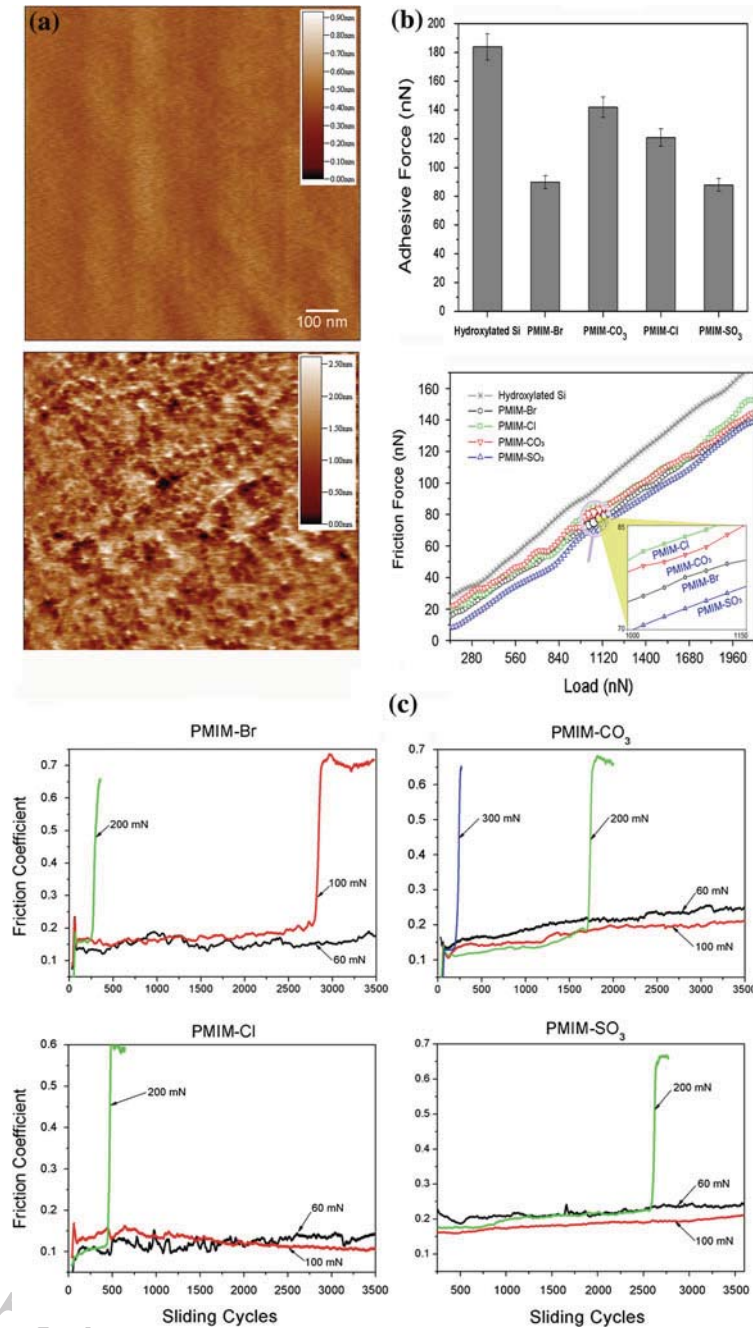


**Fig. 3.12** **a** AFM images of hydroxylated Si and IL film surfaces. **b** Adhesive and friction forces between colloidal probe and the surfaces of PMIM-Br, PMIM-CO<sub>3</sub>, PMIM-Cl and PMIM-SO<sub>3</sub> IL films. **c** Plots of friction coefficients as function of sliding cycles for PMIM-Br, PMIMOH-CO<sub>3</sub>, PMIM-Cl and PMIM-SO<sub>3</sub> film on silicon. Reproduced with permission from Ref. [49]. Copyright (2010) Surface and Interface Analysis

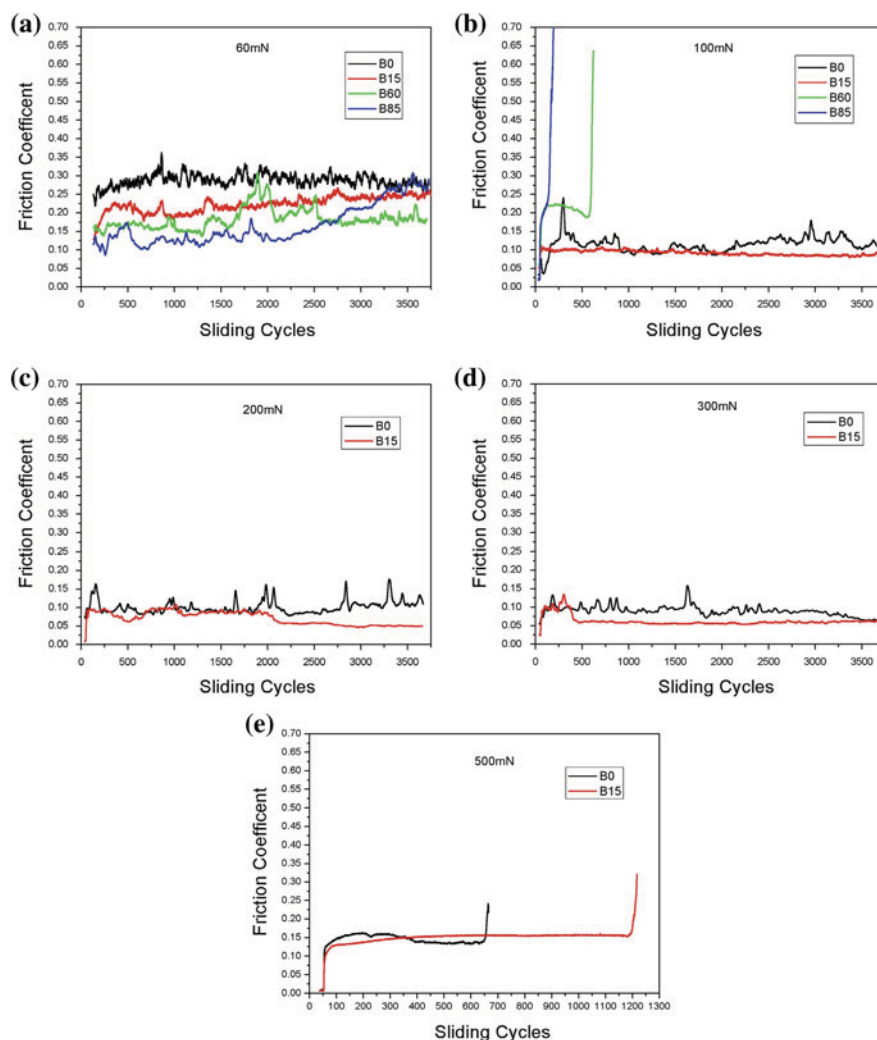


**Fig. 3.13** Plots of friction coefficient of AEIImi-Cl ionic liquid films with various bonding percentages as function of sliding cycles against steel ball at normal loads of 60, 100, 200, 300, 500 mN with a sliding velocity of 10 mm/s. (The films bonding percentages of 0, 15, 60, and 85 % were denoted as B0, B15, B60, and B85, respectively). Reproduced with permission from Ref. [44]. Copyright (2008) Elsevier B. V

453 observed that the films with higher bonding percentage exhibited a lower friction  
 454 coefficient.

455 The relationship between friction force and external loads for AEIImi-Cl ionic  
 456 liquid with various alkyl chain lengths (viz. C<sub>1</sub>, C<sub>4</sub>, C<sub>8</sub>) is shown in Fig. 3.14. In  
 457 general, friction is reduced with increase of chain length, and the C<sub>8</sub>AEIImi-Cl  
 458 ionic liquid exhibits lowest friction force compared to others. In the formation of

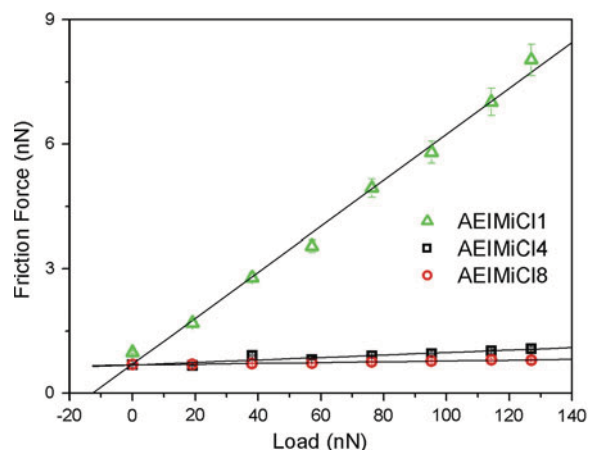


**Fig. 3.14** Plots of friction force versus applied loads for AEImi-Cl IL monolayer films with various chain lengths. Reproduced with permission from Ref. [44]. Copyright (2008) Elsevier B. V

459 the bonding coatings, both the surface energy and inter-chain interactions play  
 460 important roles and determine quality of the films. Since the AEImi-Cl is the ionic  
 461 liquid with same terminal group, the nano-friction property is determined by inter-  
 462 chain interactions.

#### 463 *Effect of Function Group and Annealing Treatment*

464 Zhao et al. [51] successfully prepared four kinds of IL films with different func-  
 465 tional cations (1-butyl-3-methylimidazolium hexafluorophosphate, 1-ethanol-  
 466 3-methylimidazolium hexafluorophosphate, 1-acetic acid -3-methylimidazolium-  
 467 hexafluorophosphate and 1-phenyl-3-methyl-imidazolium hexafluorophosphate)  
 468 and characterized their composition and microstructure. The results indicated that  
 469 IL nanofilms with polar or stiff phenyl cations exhibited relatively higher friction  
 470 force and better antiwear performance than the ones with apolar alkyl chain  
 471 structure at micro/nanoscale. The different micro/nanofriction performances of the  
 472 IL nanofilms were mainly dependent on their different cations which mainly  
 473 influence their hydrophobic/hydrophilic properties. IL films with more polarized  
 474 groups generally possessed higher surface energy and a relatively strong interaction  
 475 during the sliding, and therefore, higher adhesion and more energy loss are  
 476 expected, which lead to a higher friction force.

477 Surface morphologies and XPS results [52] indicated that different proportions  
 478 were formed after post annealing treatment (Fig. 3.15). Annealing treatment of IL  
 479 film can change the proportions of bonded and mobile molecule in the films. The  
 480 mobile lubricant fraction present in the partially bonded samples facilitates sliding  
 481 of the tip on the surfaces; it can rotate with the tip sliding direction easily and

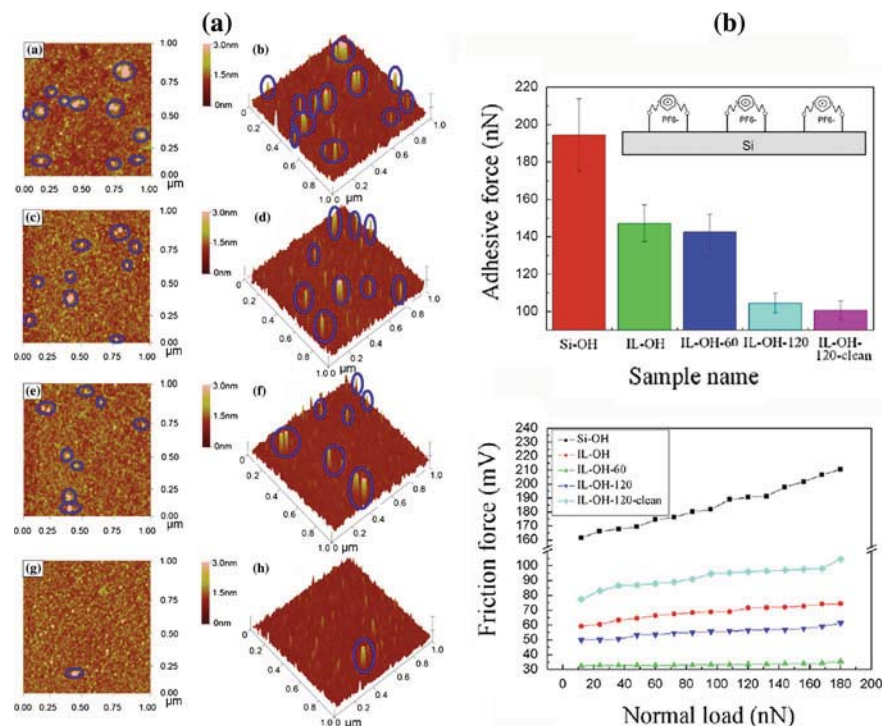


**Fig. 3.15** **a** AFM images of IL-OH film at various annealing temperature (from up to down, IL-OH film surfaces are more uniform with reduction in the number of islands); **b** Adhesive and friction force curves of Si, IL-OH films after annealing treatment. Reproduced with permission from Ref. [51]. Copyright (2010) Elsevier B. V

482 hence the film with higher mobile lubrication fraction exhibits the best nano-  
 483 tribological performance. Annealing treatment significantly changed friction and  
 484 adhesion performance at nanoscale.

### 485 *IL Films with Dual-Layer Structure*

486 Choi et al. [53] prepared mixed lubricants with dual-layer structures on a hydro-  
 487 genated amorphous carbon surface, which consist of alkylsilane SAMs and mobile  
 488 PFPE lubricants, and found that the friction and durability properties of the mixed  
 489 lubricants on the carbon surface were mainly dependent on the alkylsilane mono-  
 490 layers. In order to strengthen bonded fraction and further enhance durability of  
 491 thin IL film, Pu et al. [54] optimized reaction conditions to achieve partial bonding  
 492 of ILs to silicon substrate by acid-amide reaction between imidazolium-based ILs  
 493 carrying carboxylic functional groups and amide-containing SAMs as anchor



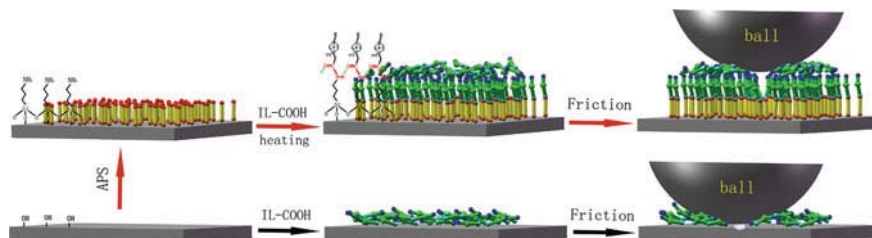


**Fig. 3.16** Schematic drawing of the constructing process and frictional mechanism of APS-IL film and IL-COOH film. Reproduced with permission from Ref. [54]. Copyright (2010) Elsevier B. V

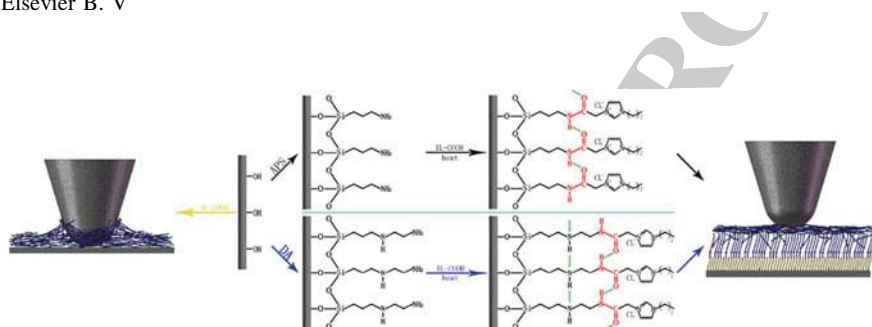


**Fig. 3.17** Schematic drawing of the construction process and nanofriction mechanism of APS-IL, DA-IL and IL-COOH films. Reproduced with permission from Ref. [54]. Copyright (2010) Colloids and Surfaces A

494 layer, and investigated influence of different self-assembled underlayer on the  
 495 tribological properties of ILs with two-phase structure, aiming to further optimize  
 496 the nanotribological behaviors of thin IL films and acquire insights into their  
 497 potential in resolving the tribological problems of MEMS (Figure 3.16).

498 As shown schematically in Fig. 3.17, a dual-layer film containing both bonded  
 499 and mobile fractions in IL-COOH layer was constructed on silicon substrates by a  
 500 two-step process. Two kinds of amino-terminated SAMs which served as anchor  
 501 layers were formed on hydroxylated silicon surfaces, respectively. Then, the  
 502 incoming IL-COOH were chemically adsorbed onto amino-terminated SAMs by  
 503 heat treatment, and formed two-phase structure composed of bonded and mobile  
 504 IL-COOH molecules.

505 The formation of chemically bonded phase in IL-COOH layer improves  
 506 nanotribological properties of the two kinds of dual-layer films as compared with  
 507 single layer IL-COOH film, which is attributed to synergic effect between mobile  
 508 phase and steady bonded phase. The protective bonded IL-COOH fraction greatly  
 509 enhances the stability and antiwear properties of the film, while the mobile  
 510 IL-COOH fraction serves as lubricant with friction reducing and self-replenish-  
 511 ment properties. Generally, the packing density of the underlayer dictates packing  
 512 density of the overlayer. N-[3-(trimethoxysilyl)propyl] ethylenediamine (DA)



513 molecules with longer chains as anchors form more densely packed and orderly  
514 SAM as compared with APS, thus more IL-COOH molecules are chemically  
515 grafted to DA anchor layer, which produce more densely packed bonded phase and  
516 reduce meniscus effect resulted from excessive mobile molecules. These charac-  
517 teristics of DA-IL lead to its lowest friction coefficient among studied dual-layer  
518 films. The improved durability of DA-IL film is closely related to high load-  
519 carrying capacity of more densely packed and ordered bonded phase. Furthermore,  
520 the more interlinked hydrogen bonding further strengthens immobile fraction of  
521 dual-layer film.

## 522 **Enhancement of Nanotribology and Wettability by Surface** 523 **Textures in Adhesion Resistant**

### 524 *Regular Surface Textures*

525 Nature often uses topographic patterning to control interfacial interactions, such as  
526 adhesion and release. Examples range from lotus leaf, gecko to jumping spider.  
527 Each example demonstrates that additional to chemistry and material properties,  
528 geometric structure is also critical for optimizing interfacial design. Although  
529 nature has provided guidance, little is known of how topographic patterns can be  
530 intelligently used not only to enhance adhesion but also more importantly to tune  
531 adhesion. To tune adhesion with patterns, we must understand how material  
532 properties and pattern structure interact. Surface textures and chemical modifica-  
533 tion are commonly used in magnetic disk drives and MEMS to reduce friction and  
534 adhesion in order to reduce the possibility of mechanical failure [55–58].  
535 A number of fabrication methods were used to generate micro/nano-hierarchical  
536 structures, including laser/plasma/chemical etching [59], soft photolithography  
537 [60], sol-gel processing and solution casting [61], electrical deposition [62], dip-  
538 pen printing [63], AFM local anodic oxidation [64], and so on.

539 Zhao et al. [65] prepared hierarchical structures by replication of textured  
540 silicon surfaces using polydimethylsiloxane (PDMS) and self-assembly of  
541 alkanethiol [ $\text{CH}_3(\text{CH}_2)_9\text{SH}$ ] to create hydrophobic surface and to improve nano-  
542 tribological properties of MEMS. As shown in Fig. 3.18, the fabrication technique  
543 is a low cost, two-step process, which provides flexibility in fabrication of various  
544 hierarchical structures. The textured surface with nano-hierarchical structures can  
545 be tailored by adjusting the depth and fractional surface coverage of cylinder hole.

546 For the adhesive force values there is a decrease when the pillar height and  
547 fractional surface coverage increases. Adhesive force also decreased greatly after  
548 chemical modification. Compared with the nanopatterned Au surface, the Au  
549 surface with micro/nanopillar textures greatly improved the adhesive properties  
550 and showed lower adhesive forces. Among the Au surfaces with textures, textured  
551 surface with the lowest height of 20 nm were fabricated, and chemical

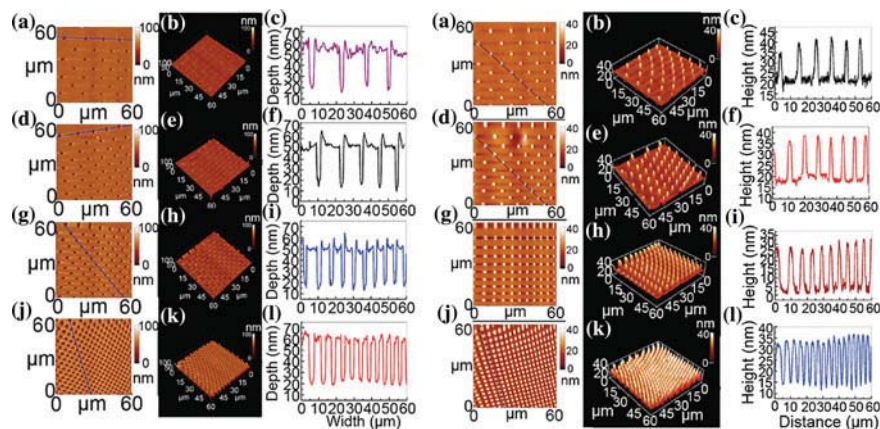


**Fig. 3.18** Surface morphologies of template and textured surfaces. Reproduced with permission from Ref. [65]. Copyright (2010) American Chemical Society

552 modification with ODT-SAMs can lower adhesive force. The results indicate that  
 553 adhesive force is closely related to the real contact area between the tip and  
 554 surface, larger area lead to increase adhesive force. With the increase in pillar  
 555 height and fractional surface coverage, the tip traveling between the pillars results  
 556 in the decrease of the contact area, responsible for decreased adhesive force.  
 557 Furthermore, when the solid surfaces were hydrophilic, they would easily form  
 558 meniscus by the adsorbed water molecules, thus they had larger adhesive force.  
 559 However, when the surfaces were hydrophobic, they would show lower adhesion  
 560 (Fig. 3.19).

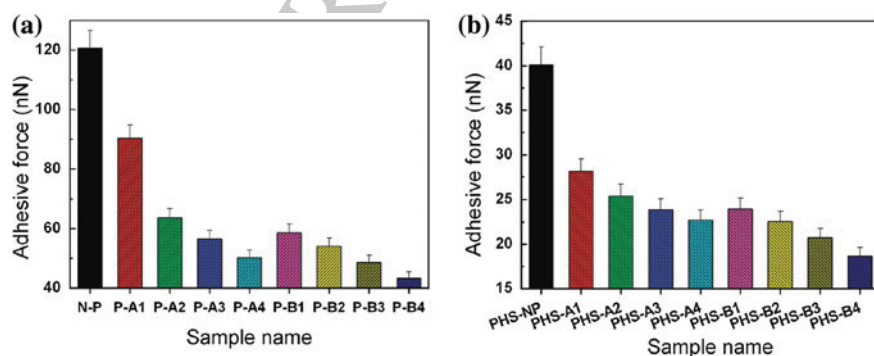


**Fig. 3.19** Adhesive forces between AFM tip and Au micro/nano patterned surfaces with different height and surface coverage **a** before and **b** after SAMs chemical modification at room temperature and a relative humidity of 30–40 %. Reproduced with permission from Ref. [65]. Copyright (2010) American Chemical Society

561 **Biomimetic Surface Textures**

562 Functional surfaces with biomimetic micro textures have aroused much interest  
563 because of their great advantages in applications such as hydrophobic, anti-  
564 adhesion etc. For example, some plant leaves and bodies of animals are known to  
565 be hydrophobic in nature because of their intrinsic geometric microstructure. In  
566 particular, lotus leaf, on which the water contact angle is larger than  $150^\circ$ , can  
567 carry effortlessly the contaminations attached to the leaf when the surface is  
568 slightly tilted, which shows self-cleaning function and low hysteresis.

569 Wang et al. [66] reported three surface micro textures of rice leaf, lotus leaf and  
570 snake skin, which were duplicated on surface by combining duplication and  
571 electroplating methods. Firstly, a cellulose film is used to replicate the surface  
572 micro textures of the biological sample to obtain a negative impression of the  
573 biomimetic textures [67, 68]. A metallic layer is electrodeposited on the top of the  
574 cellulose film. Then the positive replicas of the original living creature were  
575 obtained after removing the cellulose film. Using this method, they successfully  
576 duplicated the surface microtextures of the rice leaf, lotus leaf and the snake skin  
577 on surface and evaluated wettability of the surfaces (Fig. 3.20). Zhao et al. [69]  
578 also used a simple, efficient, and highly reproducible method for producing large-  
579 area positive and negative lotus and rice leaf topography on Au surfaces based on  
580 PDMS to enhance hydrophobicity.

581 Mo et al. [70] successfully fabricated biomimetic textures onto silicon surface  
582 by local anodic lithography. Furthermore, the dimensions of biomimetic textures  
583 can be precisely controlled by controlling pulsed bias voltage, pulse width and RH,  
584 as shown in Fig. 3.21.

585 In this approach, the surfaces of dung beetle and rice leaf were replicated on  
586 H-passivated Si surface. The experimental results show that the lowest value of the

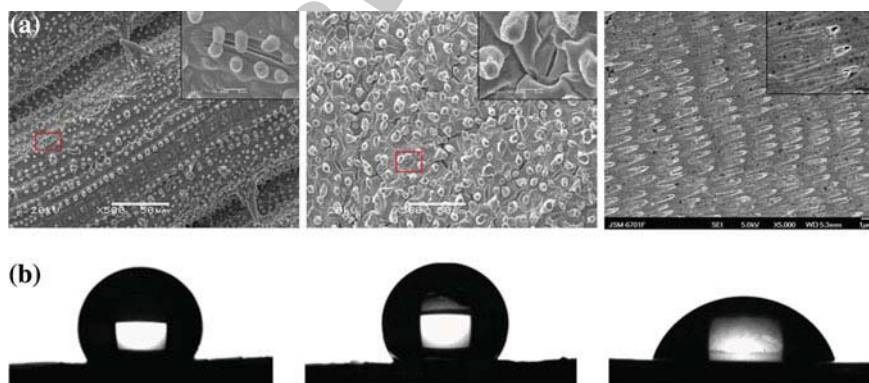


**Fig. 3.20** **a** SEM images of surface replica of rice leaf, and on surface. The insets are the high magnification images. **b** Water droplet on surface replica with different textures ( $157^\circ$  for rice leaf,  $161^\circ$  for lotus leaf and  $65^\circ$  for snake skin). Reproduced with permission from Ref. [66]. Copyright (2010) Elsevier B. V

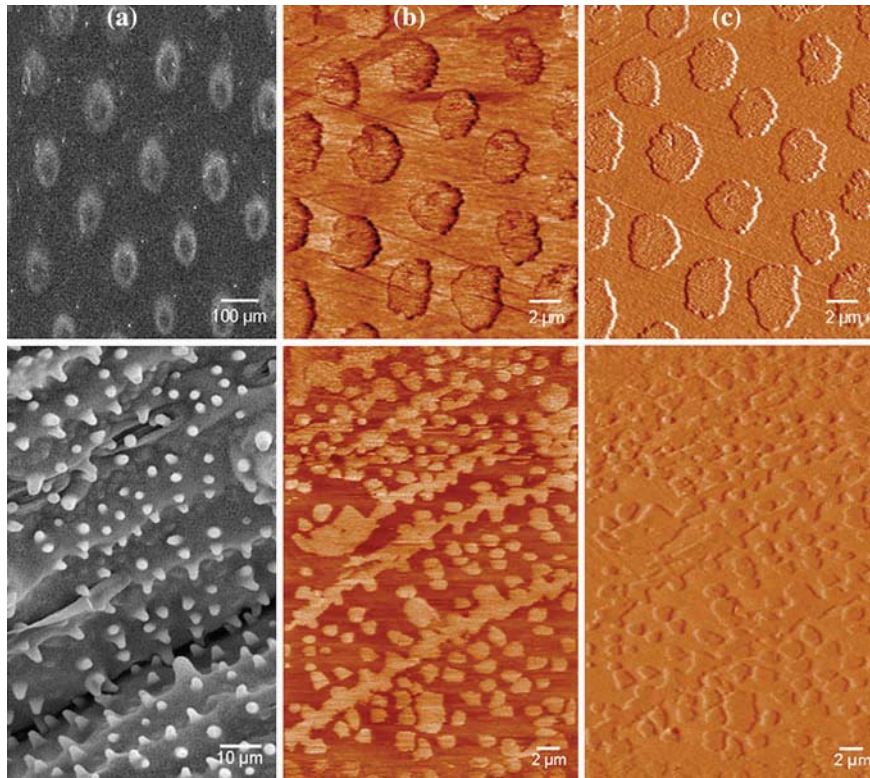
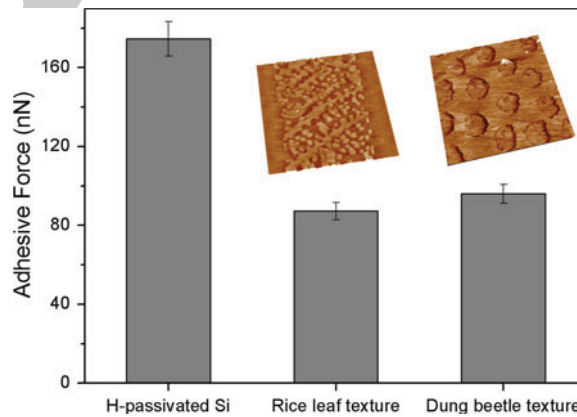


**Fig. 3.21** The SEM image **a** of the surface replica of dung beetle and rice **b** Topographic scan of the replica **c** Corresponding frictional force image of **(b)**. Reproduced with permission from Ref. [70]. Copyright (2010) Elsevier B. V

**Fig. 3.22** Adhesive forces between AFM colloidal probe and surfaces of bare H-passivated Si, rice leaf texture and dung beetle texture. Reproduced with permission from Ref. [70]. Copyright (2010) Elsevier B. V





587 height of the biomimetic nanotexture was about 1 nm. The H-passivated Si treated  
588 with biomimetic nanotextures exhibit better adhesive resistance than untreated Si  
589 at nanoscale (Fig. 3.22). It is expected that this approach could be extended to  
590 duplicate other biological and artificial template surfaces on silicon surface. These  
591 surfaces with special nanotextures are of great importance for MEMS practical  
592 applications such as microhydromechanics, wettability, and biochips.

### 593 Summary and Outlook

594 Part of the excitement in thin lubricant film is due to the great intellectual sim-  
595 plification associated with the routine way. In this chapter, we have tried to  
596 introduce those ideas and concepts. Perfluorinated SAMs have shown remarkably  
597 better lubrication and anti-adhesion properties. A comparative research is pre-  
598 sented on the surface and nanotribological properties of FC and HC SAMs on  
599 aluminum-coated silicon substrate formed by chemical vapor deposition. Fur-  
600 thermore, the influence of environmental conditions, such as RH and temperature,  
601 on tribological performance of these SAMs, was investigated. The FC SAMs show  
602 obvious environmental independence. In addition, dual-layer film exhibits better  
603 anti-wear durability than single monolayer in nanoscale.

604 MACs and ILs also are potential lubricants for MEMS and space application  
605 due to their extreme low volatility. In recent progress we have described important  
606 fields of boundary lubrication and the friction of single asperity contact. In ambient  
607 conditions, as well as in many tribological applications, surfaces are often covered  
608 by a thin film which modifies their tribological properties. Liquid menisci may  
609 form, increasing the adhesive force between the contact surfaces. The physical and  
610 chemical interactions between the surfaces are affected by the presence of water  
611 which can act as a lubricant. The tribological properties of the surface can also be  
612 changed directly by covering the surface with a monolayer of organic materials  
613 (SAMs with different function group or ILs with different ions). Meanwhile,  
614 surface texture is a prospective physical approach to enhance wettability and  
615 nanotribology in adhesion resistant conditions.

616 Summarizing, nanotribology of molecular thin films is a young and emerging  
617 field that is maturing fast, as the experiments described show. Due to never ending  
618 trend to miniaturization, understanding friction at nanoscale will become of  
619 increasing importance, since as the length scale is reduced, friction force become  
620 stronger relative to surface force, and thin films may be the only way to lubricate.  
621 If a bridge between nano- and macroscopic tribology is found, thin film with a  
622 molecular thickness might improve more efficiency and durability of MEMS.

623 **Acknowledgments** This work was funded by the National Natural Science Foundation of China  
624 (NSFC) under Grant No. 20773148, 50675217, and National 973 Program under Grant No.  
625 2007CB607601 and No. 2011CB706603. Prof. Mingwu Bai and Prof. Qunji Xue are greatly  
626 acknowledged for their constant support and encouragements to carry out this research work. The

627 authors want to express their sincere gratitude to Dr. Chongjun Pang, Dr. Jianqi Ma, Dr. Min Zhu,  
628 Dr. Wenjie Zhao, Dr. Ying Wang, Dr. Jibin Pu for their great efforts and valuable discussions.

## 629 References

- 630 1. Mo, Y., Bai, M.: *Surf. Interface Anal.* **41**, 602 (2009)
- 631 2. Hutt, D.A., Leggett, G.J.: *Langmuir* **13**, 2740 (1997)
- 632 3. Wallace, R., Chen, P., Henck, S., Webb, D.: *J. Vac. Sci. Technol. A* **13**, 1345 (1995)
- 633 4. Chance, J.J., Purdy, W.C.: *Langmuir* **13**, 4487 (1997)
- 634 5. Miura, Y.F., Takenaga, M., Koini, T., Graupe, M., Garg, N., Graham, R.L., Lee, T.R.:  
635 *Langmuir* **14**, 5821 (1998)
- 636 6. Xiao, X.D., Hu, J., Charych, D.H., Salmeron, M.: *Langmuir* **12**, 235 (1996)
- 637 7. Ren, S., Yang, S., Zhao, Y., Zhou, J., Xu, T., Liu, W.: *Tribol. Lett.* **13**, 233 (2002)
- 638 8. Ruehe, J., Novotny, V.J., Kanazawa, K.K., Clarke, T., Street, G.B.: *Langmuir* **9**, 2383 (1993)
- 639 9. Patton, S.T., William, D.C., Eapen, K.C., Zabinski, J.S.: *Tribol. Lett.* **9**, 199–209 (2000)
- 640 10. Rye, R.R., Nelson, G.C., Dugger, M.T.: *Langmuir* **13**, 2965–2972 (1997)
- 641 11. Hsu, S.M.: *Tribol. Int.* **37**, 537–545 (2004)
- 642 12. Tam-Chang, S.-W., Biebuyck, H.A., Whitesides, G.M., Jeon, N., Nuzzo, R.G.: *Langmuir* **11**,  
643 4371 (1995)
- 644 13. Clegg, R.S., Hutchison, J.E.: *J. Am. Chem. Soc.* **121**, 5319 (1999)
- 645 14. Clegg, R.S., Reed, S.M., Smith, R.K., Barron, B.L., Rear, J.A., Hutchison, J.E.: *Langmuir* **15**,  
646 8876 (1999)
- 647 15. Chambers, R.C., Inman, C.E., Hutchison, J.E.: *Langmuir* **21**, 4615 (2005)
- 648 16. Song, S., Ren, S., Wang, J., Yang, S., Zhang, J.: *Langmuir* **22**, 6010 (2006)
- 649 17. Song, S., Zhou, J., Qu, M., Yang, S., Zhang, J.: *Langmuir* **24**, 105 (2008)
- 650 18. Mo, Y., Zhu, M., Bai, M.: *Colloids Surf. A: Physicochem. Eng. Aspects* **322**, 170 (2008)
- 651 19. Ren, S.L., Yang, S.R., Zhao, Y.P.: *Langmuir* **19**, 2763 (2003)
- 652 20. Ma, J., Pang, C., Mo, Y., Bai, M.: *Wear* **2007**, 263 (1000)
- 653 21. Mo, Y., Bai, M.: *J. Phys. Chem. C* **112**, 11257 (2008)
- 654 22. Fleming, M.S., Walt, D.R.: *Langmuir* **17**, 4836 (2001)
- 655 23. Love, J.C., Estroff, L.A., Kriebel, J.K., Nuzzo, R.G., Whitesides, G.M.: *Chem. Rev.* **105**,  
656 1103 (2005)
- 657 24. Venier, C.G., Casserly, E.W.: US 4,929,782, 1990
- 658 25. Venier, C.G., Casserly, E.W.: *Lubr. Eng.* **47**, 586 (1991)
- 659 26. Dube, M.J., Bollea, D., Jones Jr, W.R., Marrchetti, M., Jansen, M.J.: *Tribol. Lett.* **15**, 3–8  
660 (2003)
- 661 27. Young, T.: *Philos. Trans. R. Soc. Lond.* **95**, 65 (1805)
- 662 28. Wang, Y., Mo, Y., Zhu, M., Bai, M.: *Tribol. Trans.* **53**, 219 (2010)
- 663 29. Ma, J., Liu, J., Mo, Y., Bai, M.: *Colloids Surf. A: Physicochem. Eng. Aspects* **301**, 481 (2007)
- 664 30. Jian, S.R., Fang, T.H., Chuu, D.S.: *J. Phys. D Appl. Phys.* **38**, 2432 (2005)
- 665 31. Garcia, R., Martinez, R., Martinezz, J.: *Chem Soc Rev* **35**, 29 (2006)
- 666 32. Mo, Y.F., Wang, Y., Bai, M.W.: *Phys. E* **41**, 146 (2008)
- 667 33. Mo, Y., Wang, Y., Pu, J., Bai, M.: *Langmuir* **25**, 40 (2009)
- 668 34. Ducker, W.A., Senden, T.J., Pashley, R.M.: *Nature* **353**, 239 (1991)
- 669 35. Hagiwara, R., Ito, Y., Fluorine, J.: *Chem.* **105**, 221 (2000)
- 670 36. Welton, T.: *Chem. Rev.* **99**, 2071 (1999)
- 671 37. Wasserscheid, P., Keim, W.: *Angew. Chem. Int. Ed.* **39**, 3772 (2000)
- 672 38. Earle, M.J., Seddon, K.R.: *Pure Appl. Chem.* **72**, 1391 (2000)
- 673 39. Nakashima, T., Kawai, T.: *Chem. Commun.* **12**, 1643 (2005)
- 674 40. Ye, C.F., Liu, W.M., Chen, Y.X., Yu, L.G.: *Chem. Commun.* **21**, 2244 (2001)
- 675 41. Liu, W.M., Ye, C.F., Gong, Q.Y., Wang, H.Z., Wang, P.: *Tribol. Lett.* **13**, 81 (2002)



- 676 42. Palacio, M., Bhushan, B.: *Adv. Mater.* **20**, 1194 (2008)  
677 43. Yu, G., Zhou, F., Liu, W.M., Liang, Y.M., Yan, S.: *Wear* **2006**, 260 (1076)  
678 44. Mo, Y., Bo, Y., Zhao, W., Bai, M.: *Appl. Surf. Sci.* **255**, 2276 (2008)  
679 45. Yu, B., Zhou, F., Mu, Z., Liang, Y.M., Liu, W.M.: *Tribol. Inter.* **39**, 879 (2006)  
680 46. Bhushan, B., Palacio, M., Kinzig, B.: *J. Colloid Interface Sci.* **317**, 275 (2008)  
681 47. Zhou, F., Liang, Y., Liu, W.: *Chem. Soc. Rev.* **38**, 2590–2599 (2009)  
682 48. Zhu, M., Yan, J., Mo, Y., Bai, M.: *Tribol. Lett.* **29**, 177 (2008)  
683 49. Mo, Y., Zhao, W., Zhu, M., Bai, M.: *Tribol. Lett.* **32**, 143 (2008)  
684 50. Sinha, S.K., Kawaguchi, M., Kato, T., Kennedy, F.E.: *Tribol. Int.* **36**, 217 (2003)  
685 51. Zhao, W., Wang, Y., Wang, L., Bai, M., Xue, Q.: *Colloids Surf. A: Physicochem. Eng.*  
686 *Aspects* **361**, 118 (2010)  
687 52. Xiao, X.D., Hu, J., Charych, D.H., Salmeron, M.: *Langmuir* **12**, 235 (1996)  
688 53. Choi, J., Kawaguchi, M., Kato, T.: *Tribol. Lett.* **15**, 353 (2003)  
689 54. Pu, J., Huang, D., Wang, L., Xue, Q.: *Colloids Surf. A: Physicochem. Eng. Aspects* **372**, 155  
690 (2010)  
691 55. Marchetto, D., Rota, A., Calabri, L., Gazzadi, G.C., Menozzi, C., Valeri, S.: *Wear* **265**, 577  
692 (2008)  
693 56. Pettersson, U., Staffan, J.: *Tribol. Int.* **36**, 857 (2003)  
694 57. Wakuda, M., Yamauchi, Y., Kanzaki, S., Yasuda, Y.: *Wear* **254**, 356 (2003)  
695 58. Suh, A.Y., Lee, S.C., Polycarpou, A.A.: *Tribol. Lett.* **17**, 739 (2004)  
696 59. Laws, G.M., Handugan, A., Eschrich, T., Boland, P., Sinclair, C., Myhajlenko, S., Poweleit,  
697 C.D.: *J. Vac. Sci. Technol. B* **25**, 2059 (2007)  
698 60. Xu, Q.B., Tonks, I., Fuerstman, M.J., Love, J.C., Whitesides, G.M.: *Nano. Lett.* **4**, 2509  
699 (2004)  
700 61. Bhushan, B., Kocha, K., Jung, Y.C.: *Soft Matter* **4**, 1799 (2008)  
701 62. Shirtcliffe, N.J., McHale, G., Newton, M.I., Chabrol, G., Perry, C.C.: *Adv. Mater.* **2004**, 16  
702 (1929)  
703 63. Zheng, Z., Daniel, W.L., Giam, L.R., Huo, F., Senesi, A.J., Zheng, G., Mirkin, C.A.: *Angew.*  
704 *Chem. Inter. Ed.* **48**(41), 7626  
705 64. Garcia, R., Martinez, R.V., Martinez, J.: *Chem. Soc. Rev.* **35**, 29 (2006)  
706 65. Zhao, W., Wang, L., Xue, Q.: *ACS Appl. Mater Interfaces* **2**, 788 (2010)  
707 66. Wang, Y., Mo, Y., Zhu, M., Bai, M.: *Surf. Coat. Technol.* **203**, 137 (2008)  
708 67. Zhao, X.M., Xia, Y., Whitesides, G.M.: *J. Mater. Chem.* **1997**, 7 (1069)  
709 68. Sun, M.H., Luo, C.X., Xu, L.P., Ji, H., Ouyang, Q., Yu, D.P., Chen, Y.: *Langmuir* **21**, 8978  
710 (2005)  
711 69. Zhao, W., Wang, L., Xue, Q.: *J. Phys. Chem. C* **114**, 11509 (2010)  
712 70. Mo, Y., Bai, M.: *J. Colloid Interface Sci.* **333**, 304 (2009)



## Author Query Form

Book ID : 214493\_1\_En  
Chapter No.: 3



Please ensure you fill out your response to the queries raised below and return this form along with your corrections

Dear Author

During the process of typesetting your chapter, the following queries have arisen. Please check your typeset proof carefully against the queries listed below and mark the necessary changes either directly on the proof/online grid or in the 'Author's response' area provided below

Query Refs.	Details Required	Author's Response
AQ1	Kindly note that Fig. 10a-e has been changed to Fig. 3.13, please check and confirm.	

UNCORRECTED PROOF